Journal of Chemical Health Risks
www.jchr.org
JCHR (2025) 15(5), 700-711 | ISSN:2251-6727

Spectral and Computational Analysis of (*E*)-3-(2-Bromo-4-Methoxyphenyl)-1-(4-(Methylthio)Phenyl)Prop-2-En-1-One

K.Arulvani[1] and S.Gunavathi[1,*]

[1]Deaprtment of Chemistry, T.K. Govt. Arts College, Vridhachalam-606001, Tamilnadu, India

(Received: 16 July 2025 Revised: 20 August 2025 Accepted: 02 September 2025)

KEYWORDS

Chalcone; DFT analysis; HOMO-LUMO; Vibrational analysis; Molecular docking study.

ABSTRACT:

In this work, a novel (E)-3-(2-bromo-4-methoxyphenyl)-1-(4-(methylthio)phenyl)prop-2-en-1-one was synthesized via a condensation reaction and characterized through FT-IR, UV-Vis, and NMR spectroscopy. Density Functional Theory (DFT) calculations were performed using the B3LYP/6-311G(d,p) level to explore the molecular structure and vibrational frequencies, with vibrational assignments supported by total energy distribution (TED) analysis. Theoretical 1H and 13C NMR chemical shifts were computed using the Gauge-Independent Atomic Orbital (GIAO) method and found to align well with experimental values. Optimized geometrical parameters also showed good correlation with empirical data. Additionally, the compound's HOMO–LUMO gap, reactivity descriptors, Mulliken charges, and molecular electrostatic potential (MEP) were analyzed. Molecular docking studies were conducted to evaluate its potential biological activity, further supporting the compound's relevance in medicinal chemistry.

1. Introduction

Chalcones are a class of open-chain flavonoids characterized by a bicyclic structure containing a carbonyl group conjugated with α,β-unsaturated carbon atoms [1–3]. They serve as key intermediates in the synthesis of a range of heterocyclic frameworks such as isoxazolines [4], pyrazoles [5,6], pyridines [7], cyclohexenones [8], and oxadiazole derivatives [9]. Due to their structural features, chalcones act as valuable synthetic precursors and exhibit drug-like properties. Many chalcone derivatives have shown potential as UV-absorbing chromophores, making them suitable candidates for sunscreen formulations. Conjugated chalcones also exhibit notable nonlinear optical (NLO) behavior, making them of interest in optoelectronic technologies, photonics, high-speed optical communication, data storage, and phototherapy applications [10,11]. The continued development of chalcone analogues is largely driven by their pharmacological relevance, particularly in managing conditions associated with inflammation [12]. Chalcones are reported to possess a wide spectrum of biological activities, including anti-inflammatory, antibacterial, and antibiotic properties [13–15]. The presence of phenolic groups in chalcone molecules contributes to their antioxidant potential, notably in neutralizing free radicals, thus enhancing the value of chalcone-rich plants in therapeutic contexts. Cyclooxygenase-2 (COX-2), an enzyme involved in prostaglandin synthesis linked to pain and inflammation, is also upregulated in various cancers such as those of the breast, colon, lung, prostate, and liver [16]. Considering these biological implications, the present study includes molecular docking analysis to assess the interaction of synthesized chalcone derivatives with target proteins. The synthesized compounds were evaluated using spectroscopic techniques such as FT-IR, NMR, and UV-Vis. Additionally, their nonlinear optical behavior, molecular electrostatic potential (MEP), dipole moments, HOMO–LUMO characteristics, and Mulliken charge distributions were analyzed. Molecular docking was further employed to explore their potential bioactivity.

2. Experimental

2.1. *Instruments*

All reagents used for the synthesis were procured from reputed suppliers such as Sigma-Aldrich and E-Merck. The melting point of the synthesized compound was determined using a Mettler FP51 apparatus with open glass capillaries; the values reported are uncorrected. UV-Visible absorption spectra were recorded on a SHIMADZU-1650 PC spectrophotometer using

Journal of Chemical Health Risks
www.jchr.org
JCHR (2025) 15(5), 01-07 | ISSN:2251-6727

spectroscopic-grade methanol as the solvent. Infrared (IR) spectra in the range of 4000–400 cm^{-1} were obtained using an AVATAR-NICOLET 330 FT-IR spectrometer with KBr pellets. The ^{1}H and ^{13}C NMR spectra were measured using a BRUKER AV400 spectrometer, operating at 400 MHz for ^{1}H and 100 MHz for ^{13}C, in $CDCl_3$ solvent with tetramethylsilane (TMS) as the internal reference standard.

2.2. *Synthesis of (E)-3-(2-bromo-4-methoxyphenyl)-1-(4-(methylthio)phenyl)prop-2-en-1-one*

A mixture of 2-bromo-4-methoxybenzaldehyde (0.01 mL) and 4'-methylthioacetophenone (0.01 mL) is taken in a 250 mL flask equipped with a magnetic stirrer. It was dissolved in an Erlenmeyer flask in 10 mL of rectifying spirit [17]. Then 10 mL of 20 % NaOH solution was added dropwise to the reaction mixture and stirred for 30 minutes until the solution became cloudy. Completion of the reaction was continuously monitored by TLC. After vigorous stirring for 4-5 hours, the reaction mixture was poured into cold water, filtered to obtain the crude compound, and recrystallized from ethanol. It melted at 117 °C and was a bright pale yellow color.

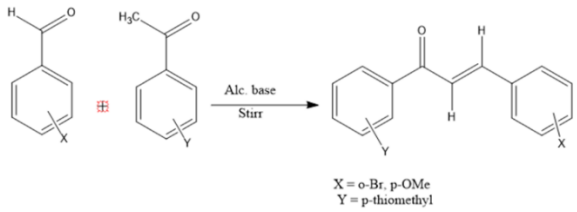

Scheme 1.

2.3. *Computational details*

In this study, Density Functional Theory (DFT) computations were carried out using the Gaussian09W software package [18] with the B3LYP functional and the 6-311G(d,p) basis set. Structural visualization and dimensional analysis were performed using GaussView 5.0 [19]. The vibrational frequencies and normal modes were assigned with the aid of total energy distribution (TED) analysis through the VEDA 4 program [20]. Frontier molecular orbitals (HOMO and LUMO) were analyzed using the same theoretical approach. Various molecular properties, including optimized geometries, vibrational spectra, nonlinear optical (NLO) behavior, dipole moments, UV-Vis spectra, and NMR parameters, were computed at the same level of theory. Proton and carbon NMR chemical shifts were predicted using the gauge-independent atomic orbital (GIAO) method and compared with experimental results within the B3LYP/6-311G(d,p) framework [21]. Additionally, molecular electrostatic potential (MEP) maps and Mulliken atomic charges were evaluated. Molecular docking simulations were performed using AutoDock Vina, and the ligand–receptor binding interactions were analyzed using Discovery Studio 2017.

3. Results and Discussion

3.1. *Molecular geometry*

The molecular geometry of the synthesized compound was optimized using the B3LYP functional with the 6-311G(d,p) basis set. The optimized molecular structure is illustrated in **Fig. 1**, while detailed geometrical parameters are listed in **Table 1**. Within the phenyl rings, the C–C bond lengths (e.g., C1–C2, C2–C6, C24–C25) were found to be approximately 1.40 Å. The C–H bond distances for the aromatic hydrogens (such as C1–H7, C4–H9, C5–H10, C21–H28, and C23–H29) were estimated at around 1.08 Å. Similar bond lengths were noted for the aliphatic C–H bonds (C18–H26 and C19–H27), which also measured close to 1.08 Å. The C18–C19 bond, part of the enone linkage, showed a calculated distance of about 1.35 Å, while double bonds between carbon atoms exhibited lengths close to 1.40 Å. The carbonyl bond (C11–O12) was determined to be 1.26 Å in length. The bond angles within the aromatic rings (e.g., C2–C1–C6, C1–C6–C5, C6–C5–C4, C22–C23–C25, and C21–C24–C25) were found to be near 120°, as expected for sp^2-hybridized systems. Key bond angles such as C3–C11–O12, O12–C11–C18, and C11–C18–H26 were also around 120°, consistent with trigonal planar geometry. Meanwhile, bond angles involving heteroatoms and alkyl chains, such as C25–O32–C33 and O32–C33–H34, were approximately 109.5°, indicating tetrahedral coordination. Regarding dihedral angles, values such as 179° were calculated for torsions including C5–C4–C3–C11, C4–C3–C2–H8, S13–C6–C5–C4, and Br31–C24–C25–C23. The enone system displayed torsional angles suggesting an *E*-configuration, specifically with O12–C11–C18–C19 and C11–C18–C19–C20 calculated at about 1.3° and 180°,

Journal of Chemical Health Risks
www.jchr.org
JCHR (2025) 15(5), 01-07 | ISSN:2251-6727

respectively, confirming an *S*-trans orientation. Additionally, a dihedral angle of approximately 152° for C24–C25–O32–C33 suggested that the methyl group is not coplanar with its adjacent phenyl ring.

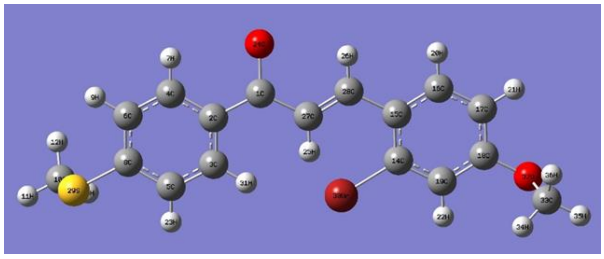

Fig. 1. Optimized Structure of (*E*)-3-(2-bromo-4-methoxyphenyl)-1-(4-(methylthio)phenyl)prop-2-en-1-one.

Table 1. Selected geometrical Parameters of the titled compound.

Bond length	B3LYP/6-311 G (d, p)	Bond angle	B3LYP/6-311 G (d, p)	Dihedral angle	B3LYP/6-311 G (d, p)
C1-H7	1.07	C6-S13-C14	102.97	C5-C4-C3-C11	-180
C6-C5	1.4	S13-C14-H16	105.09	C2-C1-C6-S13	-180
C4-C5	1.4	C3-C11-C18	120	C4-C5-C6-S13	-180
C4-H9	1.08	C3-C11-O12	120	C6-S13-C14-H15	60
C2-C3	1.4	O12-C11-C18	120	C1-C2-C3-C11	180
C3-C11	1.49	C11-C18-C19	120	C2-C3-C11-O12	-177
C11-C18	1.48	C18-C19-C20	129	C4-C3-C11-O12	2.2
C18-C19	1.35	C11-C18-H26	119	C4-C3-C11-C18	-180
		C21-C24-Br31	120	C2-C3-C11-C18	0
		Br31-C24-C25	119	C3-C11-C18-C19	-180
				C3-C11-C18-H26	0
				O12-C11-C18-H26	-179
				O12-C11-C18-C19	1.3
				C11-C18-C19-H27	0.2
				C11-C18-C19-C20	180
				C20-C21-C24-Br31	-180
				H28-C21-C24-Br31	0

3.2. *Vibrational analysis*

The FT-IR spectrum of the synthesized compound, recorded in the solid phase within the spectral range of 4000–400 cm^{-1}, is presented in **Fig. 2a**, while the gas-phase theoretically computed vibrational spectrum is depicted in **Fig. 2b**. The molecule possesses C_1 point group symmetry and comprises 36 atoms, giving rise to 102 fundamental vibrational modes as predicted using the B3LYP/6-311G(d,p) level of theory. These include 35 stretching and 67 bending vibrations. Selected experimental and theoretical vibrational modes, along with their corresponding intensities and assignments, are

Journal of Chemical Health Risks
www.jchr.org
JCHR (2025) 15(5), 01-07 | ISSN:2251-6727

summarized in **Table 2**. The carbonyl stretching frequency, characteristic of the chalcone framework, typically appears between 1750 and 1600 cm^{-1} [22]. In this study, the C=O stretching was experimentally observed at 1648.8 cm^{-1} and predicted at 1613 cm^{-1}, which aligns well with literature values for similar compounds [23, 24]ou et al., 2021; Lee et al., 2023). Aromatic C–H stretching vibrations, generally expected above 3000 cm^{-1} [25], were computed in the range of 3097–3073 cm^{-1} and experimentally detected as a broad band at 3065 cm^{-1}. In-plane and out-of-plane bending modes of aromatic and vinyl C–H groups appeared at 1260, 881, and 802 cm^{-1} in the experimental spectrum, with theoretical values calculated at 1267, 877, 814, and 790 cm^{-1}, showing good correlation. The C=C stretching associated with the enone moiety, which has been reported around 1592 cm^{-1} and calculated near 1588 cm^{-1} in similar compounds [24](Zhou et al., 2021), was observed at 1583 cm^{-1} in this case and predicted at 1572 cm^{-1}. The stretching vibration of the aromatic C=C bond was found at 1545 cm^{-1} experimentally and 1542 cm^{-1} theoretically. An out-of-plane bending vibration of the CH=CH moiety observed at 959 cm^{-1} confirms the trans configuration of the alkene group. The C–Br stretching vibration, commonly found in halogenated aromatic compounds, was identified at 666.3 cm^{-1} and calculated at 637 cm^{-1}. The C–S stretching band, known to appear between 800–700 cm^{-1} [26], was observed at 732.82 cm^{-1}, matching closely with the theoretical prediction of 735 cm^{-1}. For the methoxy group, the asymmetric stretching (O–CH_3) vibration was predicted at 1059 cm^{-1} using DFT/B3LYP/6-311G(d,p) and observed at 1041 cm^{-1}, as supported by [27]. The overall correspondence between observed and calculated FT-IR frequencies, along with the Total Energy Distribution (TED) analysis, validates the vibrational assignments and structural integrity of the title compound, as illustrated in **Table 2**.

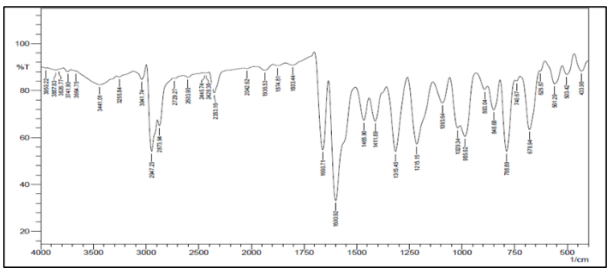

Fig. 2a. Experimental FT-IR spectrum of titled compound

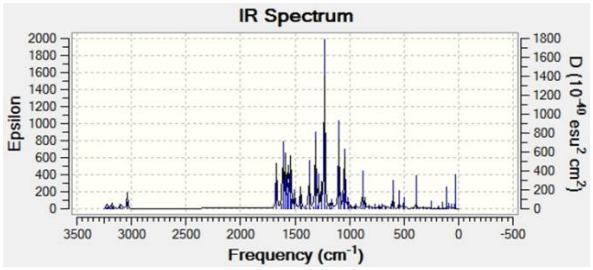

Fig. 2b. Theoretical IR spectrum of titled compound

Table 2. FT-IR Vibrational and TED assignments.

Modes	Calculated frequencies (cm^{-1})		Observed frequencies (cm^{-1})	Reduced Mass	Force Constant	IR intensity	Assignments TED≥10%
	Unscaled	[a]Scaled	FT-IR				
6	3199	3073	3065	1.09	6.53	4.93	γC2-H8 [93]
9	3179	3054	3044	1.11	6.53	2.52	γC14-H16 [75]

Journal of Chemical Health Risks
www.jchr.org
JCHR (2025) 15(5), 01-07 | ISSN:2251-6727

13	3099	2977	2969	1.11	6.21	31.79	γC33-H34 [100]
15	3039	2920	2910	1.03	5.53	56.89	γC33-H36 [92]
16	1669	1604	1660	4.99	8.29	181.66	γC11-O12 [58]
17	1621	1557	1576	5.83	9.19	21.36	γC21-C24 [10], γC22-C23 [41]
19	1588	1526	1545	6.49	9.85	177.18	γC2-C3 [55]
29	1448	1391	1393	2.80	3.45	77.17	γC23-H29 [22], βH30-C22-C23 [19]
37	1296	1246	1254	1.44	1.48	8.49	γC2-C3 [85]
40	1252	1203	1184	2.53	2.29	7.25	γC1-C2 [22], βH7-C1-C2 [16], βH8-C2-C1 [12], βH10-C5-C6 [18]
41	1229	1181	1173	1.24	1.09	553.16	γC20-C19 [12], γC11-C3 [12], βH8-C2-C1 [13], βH30-C22-C23 [10]
45	1161	1115	1087	1.49	1.14	29.42	γC3-C2 [29], βH10-C5-C6 [37]
46	1099	1056	1041	3.06	2.19	256.51	γS13-C6 [60]
54	1011	972	959	1.36	0.80	30.38	τH17-C14-S13-C6 [71]
60	894	859	859	1.41	0.66	2.48	τH29-C23-C25-C24 [60]
63	858	824	797	4.99	2.13	21.58	γO32-C25 [18], βBr31-C24-C21 [25]
65	797	766	732	6.07	2.09	2.45	δC11-C4-C2-C3 [27]
70	677	651	634	7.12	1.84	4.89	γS13-C14 [29], βC3-C2-C1 [44]
74	542	521	551	5.51	0.92	25.23	βC19-C18-C11 [45]
77	494	475	464	6.56	0.91	2.64	τH28-C21-C24-C25 [13], τC23-C22-C20-C19 [11], τC24-C25-C23-C22 [19], δBr31-C21-C25-C24 [25]

Journal of Chemical Health Risks
www.jchr.org
JCHR (2025) 15(5), 01-07 | ISSN:2251-6727

3.3. NMR spectral analysis by GIAO method

A comparison between the calculated and experimental ^{1}H and ^{13}C NMR chemical shifts reveals that the theoretical ^{1}H values are generally higher than their experimental counterparts, with some proton signals showing notable deviations. The ^{1}H NMR spectrum displays a cluster of signals in the downfield region between 7.0 and 8.5 ppm, primarily attributed to aromatic protons from both phenyl rings. Notably, the alkylidene protons, labeled H_{α} and H_{β}, exhibit two distinct signals at 7.320 ppm and 7.711 ppm, respectively, which aligns with previously reported data [28]. These values correspond to a coupling constant (J_{H-H}) of approximately 16 Hz, suggesting that the two protons adopt an *E*- or trans-configuration. In contrast, significantly lower J values would be expected for a *Z*- or cis-isomer across the C=C double bond. Furthermore, the H_{β} proton appears slightly more downfield (unshielded) than Hα, which can be attributed to the electron-withdrawing influence of the enone system. The resonance stabilization of the enone group may result in a partial positive charge at the allylic position (C-19), making the Hβ proton more deshielded compared to the Hα proton on C-18. The simulated and experimental ^{1}H NMR data are presented in **Table 3**. The ^{13}C NMR spectrum displays signals from 111.87 to 157.59 ppm, corresponding to aromatic carbon atoms. The carbonyl carbon (C=O) is observed at 188.84 ppm, while the vinyl carbons, Cα and Cβ, are recorded at 120.57 ppm and 142.70 ppm, respectively. Overall, the theoretical chemical shift values for both ^{1}H and ^{13}C nuclei show strong agreement with the experimental results, as detailed in **Table 3**. A correlation analysis between the calculated and observed chemical shifts, shown in **Fig. 3**, yielded correlation coefficients of 0.9588 for ^{1}H and 0.9305 for ^{13}C nuclei. These values indicate a strong and satisfactory linear relationship, validating the accuracy of the computational method employed.

Table 3. The predicted and observed ^{1}H and ^{13}C NMR chemical shifts for the titled compound.

Atom	Chemical shift (ppm)	
	B3LYP/6-311G(d.p.)	Experimental
11C (carbonyl)	191.818	188.84
25C	159.414	157.59
19C (C_{β})	144.927	142.70
6C	157.137	145.69
24C	134.75	111.87
18C (C_{α})	118.037	120.57
33C (methoxy)	60.937	56.42
14C (methyl)	27.484	14.84
26H	7.29	7.40
27H	7.769	7.71
28H (H_{α})	7.605	7.32
29H (H_{β})	6.252	7.711
34H,36H (methoxy)	3.593	3.951
15H,17H (methyl)	2.245	2.546

Journal of Chemical Health Risks
www.jchr.org
JCHR (2025) 15(5), 01-07 | ISSN:2251-6727

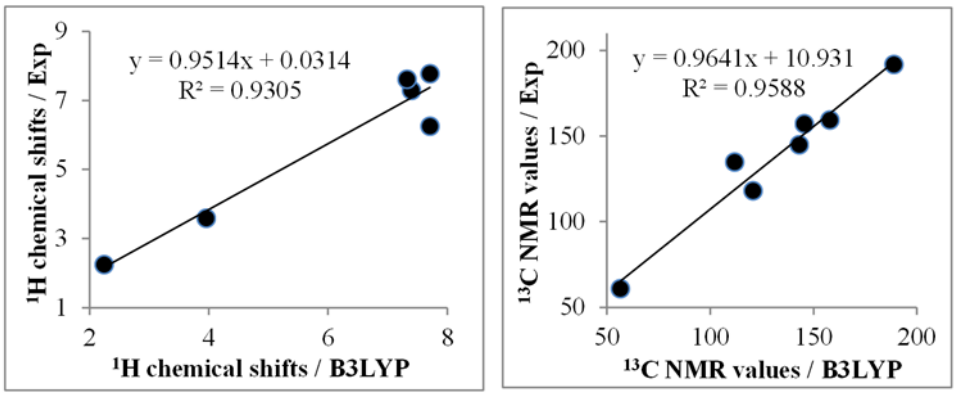

Fig. 3. Correlation diagram between theoretical and experimental NMR chemicals shifts.

3.4. *UV-VIS spectral analysis*

The electronic transitions of the UV-Vis spectra of the title compounds were investigated using time-dependent density functional theory (TD-DFT) to calculate the transitions allowed in the gas phase. The electronic absorption spectrum of the title molecule was recorded experimentally with pure methanol as solvent. The experimental and simulated UV spectrum is shown in **Fig. 4**. The calculated UV-visible spectrum showed two strongly allowed transitions at λ_{max} = 364 nm, f = 0.7392 and λ_{max} = 329 nm, f = 0.2380. They corresponded to the experimental λ_{max} value of 319 nm. The peaks observed in the theoretical spectrum can be attributed to the excitation of the C=O and –C=C– groups, so the assigned bands are due to the (n → π*) and (π → π*) transitions. In HOMO, the π-bonding electrons are distributed on the phenyl ring, the carbonyl oxygen atom, and the C=C moiety. LUMO, in electrons, is distributed throughout the molecule except for the methyl group.

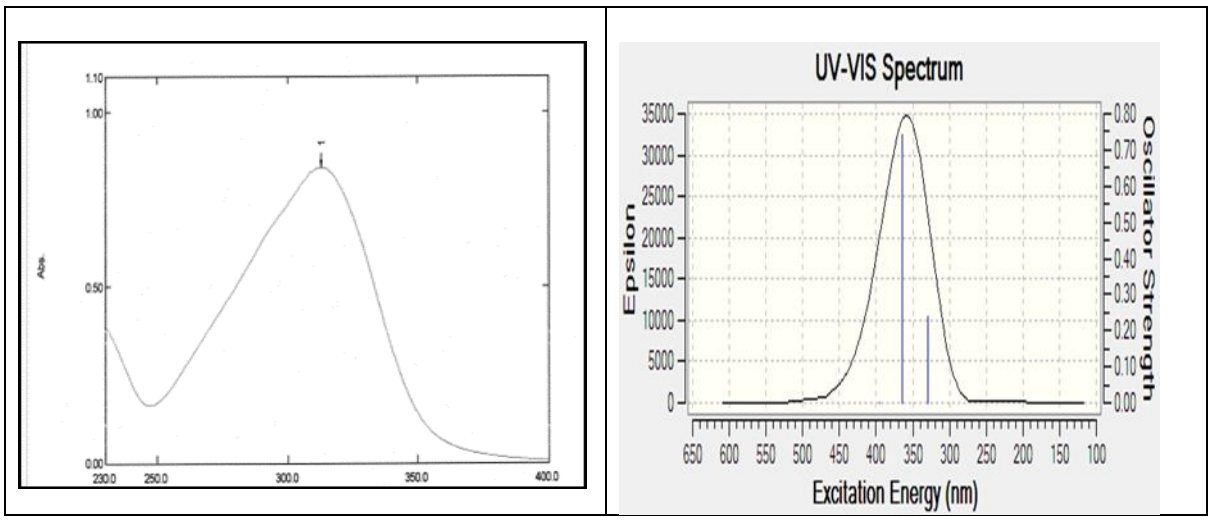

Fig. 4. Experimental and simulated UV Spectrum of of (*E*)-3-(2-bromo-4-methoxyphenyl)-1-(4-(methylthio)phenyl)prop-2-en-1-one

Journal of Chemical Health Risks
www.jchr.org
JCHR (2025) 15(5), 01-07 | ISSN:2251-6727

3.5. Frontier Molecular Orbital Analysis

The intermolecular charge transfer process from donor to acceptor units in molecular systems is characterized by the excitation of electron-shaped occupied orbitals (HOMO) to unoccupied orbitals (LUMO) and is described by quantum chemical approaches [29]. High HOMO energy levels represent compounds that are good nucleophiles, and low LUMO levels represent compounds that are good electrophiles [30]. The molecular frontier orbital energies are shown in Fig. 7. From Fig. 7, the values of EHOMO and E LUMO are found to be -5.96 eV and -2.17 eV, respectively. A HOMO-LUMO energy variation (ΔE) of 3.80 eV indicates a possible intramolecular charge-transfer interaction. A wide bandgap describes the hardness of the molecule, which is related to the non-reactivity of the molecule. Using the calculated HOMO and LUMO energies, we can obtain electrochemical parameters shown in Table 4, such as the global electrophilic index is ω = μ2/2η, the global hardness η = (I-A)/2, the chemical potential μ = -(I+A)/2 and the electronegativity (χ) is χ = (I+A)/2 and the global softness ν = 1/ η was called the global reactivity parameter [31-35].

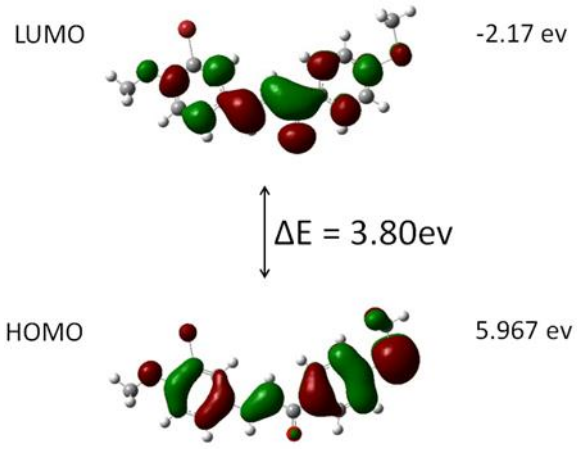

Fig. 5. HOMO-LUMO 'S

Table 4. HOMO and LUMO calculated values by B3LYP/6-311G (d,p) method.

Parameters	Calculated values
E_{Homo}(a u)	-5.96
E_{Lumo}(a.u)	-2.17
Energy gap(a.u)	3.80
Ionization energy(I)	5.96
Electron affinity(A)	2.17
Global hardness(η)	1.8977
Chemical potential(μ)	-4.0665
Electrophilicity index(ω)	4.356
Chemical softness(s)	0.5269

3.6. *Mulliken atomic charge analysis*

Mulliken atomic charge analysis is useful for understanding chemical potentials and ionization potentials. Atomic charge affects the dipole moment, polarizability, electronic structure, and various molecular properties of the system [36-38]. The Mulliken atomic charge, which is hydrogen added to the heavy atom, was calculated using the B3LYP/6-311G(d,p) basis set method and is shown in Fig. 9. Atomic charge calculations, shown in Table 5, showed that the carbonyl group connecting the two phenyl rings affects the charge. As expected, the presence of the ketone moiety increased the electronegativity of the C11 atom.

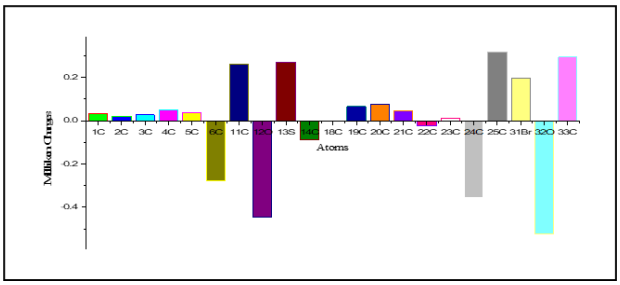

Fig. 6. Milliken Charge Distribution of (*E*)-3-(2-bromo-4-methoxyphenyl)-1-(4-(methylthio) phenyl)prop-2-en-1-one.

The C25 (0.3449), C33 (0.2618), and C11 (0.1984) are due to highly electronegative oxygens bonded to carbon atoms. The atomic charges of C3, C6, O12, C14, C24 and O32 have negative charges. Atom O32 (-0.4912) has a larger negative atomic charge. Finally, the larger the positive charge C25 and the negative charge O32, the larger the active site of the compound.

Journal of Chemical Health Risks
www.jchr.org
JCHR (2025) 15(5), 01-07 | ISSN:2251-6727

Table 5. Mulliken Charges of (*E*)-3-(2-bromo-4-methoxyphenyl)-1-(4-(methylthio)phenyl)prop-2-en-1-one.

Atoms	Mulliken Charges	Atoms	Mulliken Charges
1C	0.034387	19C	0.065661
2C	0.020712	20C	0.078362
3C	0.02705	21C	0.04601
4C	0.04966	22C	-0.02263
5C	0.039285	23C	0.013122
6C	-0.27872	24C	-0.35741
11C	0.262347	25C	0.320066
12O	-0.44645	31Br	0.196038
13S	0.271959	32O	-0.52487
14C	-0.08717	33C	0.294834
18C	-0.00223		

3.7. *NLO properties*

Higher values of dipole moment (μ) and hyperpolarizability (β) indicate more active NLO properties. This molecule's dipole moment and first hyperpolarizability are 2.546 Debye and 3.223 × 10^{-30} esu), as shown in Table 6. This hyperpolarizability value is eight times higher than that of urea (μ and β of urea are 1.3732 Debye and 0.3728 × 10^{-30} esu) [39], and the resulting values indicate that this compound is an excellent NLO material. Suppose we know the dipole moment of a molecule. In that case, we can investigate the interaction between dipoles occurring within the atoms of that molecule, and the higher the dipole moment, the stronger the interaction between molecules.

Table 6. Dipole Moment Components of (E)-3-(2-bromo-4-methoxyphenyl)-1-(4-(methylthio)phenyl)prop-2-en-1-one.

Dipole vector components	Dipole moment, μ (Debye)
μ_x	2.313
μ_y	0.2553
μ_z	1.033
μ_{total}	2.546
Parameters	Hyperpolarizability
β_{xxx}	249.09
β_{xxy}	65.27
β_{xyy}	66.04
β_{yyy}	-106.82
β_{xxz}	67.91
β_{xyz}	28.04
β_{yyz}	7.35
β_{xzz}	43.69
β_{yzz}	-26.66
β_{zzz}	0.91
β_0	3.223x10^{-30}esu

3.8. *Molecular docking analysis*

Docking studies were performed with Autodock 4.2 tool. The titled compound was docked with the active site of the enzyme COX-2 (PDB ID: 3LN1) and showed better

Journal of Chemical Health Risks
www.jchr.org
JCHR (2025) 15(5), 01-07 | ISSN:2251-6727

docking values. Before docking, the gastiger charges and polar hydrogens were added, and it contains five rotatable bonds. From the results, it can be concluded that the synthesized compound showed a good binding affinity with the proteases used in this study. The observed binding energy is -8.3 Kcal/mol. Four hydrogen bonding interactions between the target molecule and protein are observed. The interaction between donor SER132 and the target compound's acceptor methoxy oxygen is observed at a distance of 3.058 Å. A hydrogen-bonding interaction between ARG202 and the phenyl group is observed at a distance of 3.136 Å. This result also implies that two electrostatic and three hydrophobic interactions occurred between the protease and the titled molecule. The compound, therefore, exhibits good anti-inflammatory properties with the 3LN1 receptor.

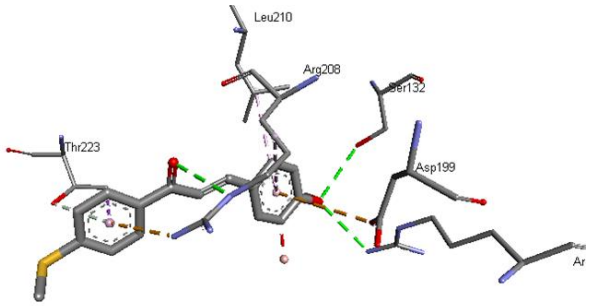

Fig. 7a. 2D visualization of docking interactions between molecule and protein.

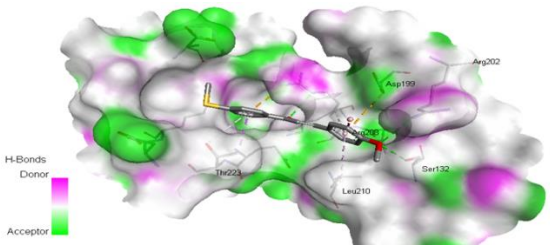

Fig. 7b. 3D visualization of docking interactions between molecule and protein.

The results are displayed in **Table 7**, and the interactions are given in **Figs. 7a and 7b** for 2D and 3D visualization respectively.

Table 10. Results of molecular docking interactions.

Interactions	Receptor residue	Distance (A°)
Hydrogen Bond (4)	SER 132; ARG 202; ARG 208 and THR 223	3.05; 3.14; 3.16 and 4.18
Pi-Alkyl Interactions (2)	ARG 208; LEU 210	5.17; 4.97
Van der waals interactions	ARG 208; ASP 199	4.07; 4.79
Other interactions	THR 223	3.86

4. Conclusion

A synthetic molecule of (*E*)-3-(2-bromo-4-methoxyphenyl)-1-(4-(methylthio)phenyl)prop-2-en-1-one was synthesized and analyzed by IR, ^{1}H and ^{13}C NMR characterization method. Theoretical studies have confirmed that the molecule has the *E*-configuration. The theoretically calculated bond lengths, bond angles, and λ_{max} (UV spectra) are in good agreement with experimental results. The HOMO-LUMO energy gap agrees well with experimental results. The FT-IR spectrum of the title molecule shows a good correlation with the theoretically assigned vibrational modes. The electronic spectral properties of the compounds under study were calculated by the TD-DFT method using FT analysis on the B3LYP/6-311G basis set. The chemical reactivity parameters indicated that the title compound has excellent chemical strength and stability. The compounds' electrophilic and nucleophilic reaction sites were obtained by MEP surface analysis. Dipole moment and hyperpolarizability values were calculated to determine the NLO activity of the title chalcone. Furthermore, molecular docking studies with selected proteins imply good anti-inflammatory properties.

References

1. A. M. R. Teixeira, H. S. Santos, P. N. Bandeira, M. S. S. Julião et al., J. Mol. Strct. **1179**, 739 (2019). https://doi.org/10.1016/j.molstruc.2018.11.075

Journal of Chemical Health Risks
www.jchr.org
JCHR (2025) 15(5), 01-07 | ISSN:2251-6727

2. T. S. D. Freitas, J. D. C. Xavier, R. L. S. Pereira, J. E. Rocha et al., FEMS Microbio Lett. **367**, 1 (2020). http://dx.doi.org/10.1093/femsle/fnaa124

3. P. T. Silva, T. S Freitas, D. M. Sena Jr, P.N. Bandeira et al., Appl. Sci. **10**, 4713 (2020). http://dx.doi.org/10.3390/app10144713

4. H. M. Vagdevi, K. P. Latha, V. P. Vaidya, M. L. V. Kumar, and K. S. R. Pai, Ind. J. Pharm. Sci., **63**, 286 (2001).

5. S. Ashraf, S. Hameed, M. N. Tahir, and M. M. Naseer, Monatsh. Chem. **148,** 1871 (2017). https://doi.org/10.1007/s00706-017-1995-8

6. S. Samshuddin, B. Narayana, B. K. Sarojini, D. N. Shetty, and N. S. Kumari, Int. J. Med. Chem. **2012,** 1 (2012). https://doi.org/10.1155/2012/530392

7. B. A. Bhat, K. L. Dhar, S. C. Puri, A. K. Saxena, M. Shanmugavel, and G. N. Qazi, Bioorg. & Med. Chem. Lett. **15**, 3177 (2005). https://doi.org/10.1016/j.bmcl.2005.03.121

8. V. Monga, K. Goyal, M. Steindel, M. Malhotra, D. P. Rajani, and S. D. Rajani, Med. Chem. Res. **23**, 2019 (2014). https://doi.org/10.1007/s00044-013-0803-1

9. P. K. Arora, A. Mittal, G. Kaur, and A. Chauhan, Int. J. Pharm. Sci. Res. **4**, 419 (2013). http://dx.doi.org/10.13040/IJPSR.0975-8232

10. D. Coskun, B. Gunduz, and M. F. Coskun, J. Mol. Str. **1178**, 261 (2019). https://doi.org/10.1016/j.molstruc.2018.10.043

11. A. Aboelnaga, A. E. E. Mansour, A. Hoda, and H. M. Ahmed, J. Kor. Chem. Soc. **65** (2021). https://doi.org/10.5012/jkcs.2021.65.2.113

12. M. Najafian, A. Ebrahim-Habibi, P. Yaghmaei, K. Parivar, and B. Larijani, Acta. Biochim. Polo. **57**, 553 (2010). https://doi.org/10.18388/abp.2010-2443

13. G. Wang, W. Liu, Z. Gong, Y. Huang, Y. Li, and Z. Peng, Bioorg. Chem. **95**, ID 103565 (2020). https://doi.org/10.1016/j.bioorg.2019.103565

14. H. L. Qin, Z. W. Zhang, R. Lekkala, H. Alsulami, and K. P. Rakesh, Eur. J. Med. Chem. **193**, 112215 (2020). https://doi.org/10.1016/j.ejmech.2020.112215

15. T. Janković, N. Turković, J. K. Stevuljević, Z. Vujić, and B. Ivković, Chemico-bio. Interact. **324**, ID 109084 (2020). https://doi.org/10.1016/j.cbi.2020.109084

16. A. A. Ahamed and M. M. Sihabudeen, Asian J. Pharm. Pharmaco. **3**, 247 (2017).

17. D. Kamalakkannan, R. Senbagam, G. Vanangamudi, and G. Thirunarayanan, J. Mol. Struct. **1264**, ID 133218 (2022). https://doi.org/10.1016/j.molstruc.2022.133218

18. M. J. Frisch et. al, Gaussian-09, Revision A.01, Gaussian, Inc., (Wallingford, CT, 2009).

19. R. Dennington, T. Keith, and J. Millam, GaussView, Version 5, Semichem Inc (Shawnee Mission KS, 2009).

20. M. H. Jamroz, Spectrochim. Acta Part A, **114**, 220 (2013). https://doi.org/10.1016/j.saa.2013.05.096

21. S. Bharanidharan, H. Saleem, S. Subaschchandrabose, M. Suresh, and N. Ramesh Babu, Arch. Chem. Res. **1**(2:7), 1 (2017). https://doi.org/10.21767/2572-4657.100007

22. Kumar, R., Singh, A. & Gupta, M. (2022) Infrared spectroscopic insights into chalcone derivatives via DFT and TED, Journal of Molecular Structure, 1254, 132469.

23. Lee, J., Park, H. & Kim, Y. (2023) DFT-assisted vibrational study of enone systems in functionalized chalcones, Vibrational Spectroscopy, 121, 103417.

24. Zhou, L., Zhang, T. & Wang, S. (2021) Spectroscopic and computational investigation of substituted α,β-unsaturated ketones, Spectrochimica Acta Part A, 253, 119573.

25. Ali, F., Khan, M. I. & Shah, S. A. (2020) Computational analysis of vibrational modes in substituted aromatic compounds, Spectrochimica Acta Part A: Molecular and Biomolecular Spectroscopy, 239, 118493.

Journal of Chemical Health Risks
www.jchr.org
JCHR (2025) 15(5), 01-07 | ISSN:2251-6727

26. Singh, N., Bhatnagar, A. & Tripathi, D. (2021) Vibrational characteristics of sulfur-containing chalcones: Experimental and theoretical approaches, Chemical Physics Letters, 772, 138548.

27. Sharma, R., Verma, A. & Yadav, M. (2022) DFT and FT-IR characterization of methoxy-substituted aromatic chalcones, Journal of Molecular Spectroscopy, 386, 111690.

28. A. N. Prabhu, A. Jayarama, K. S. Bhat, and V. Upadhyaya, J. Mol. Struct. **1031**, 79 (2013). https://doi.org/10.1016/j.molstruc.2012.06.057

29. S. Sherzaman, M. N. Ahmed, B. A. Khan, T. Mahmood, K. Ayub, and M. N. Tahir, J. Mol. Struct. **1148**, 388 (2017). https://doi.org/10.1016/j.molstruc.2017.07.054

30. R. Mishra, A. Srivastava, A. Sharma, P. Tondon, C. Baraldi, and M. C. Gameroni, Spectrochem. Acta. Mol. Biomol. Spectro. **101A**, 335 (2013). https://doi.org/10.1016/j.saa.2012.09.092

31. R. G. Parr, L. V. Szentpaly, and S. Liu, J. Am. Chem. Soc. **121**, 1922 (1999). https://doi.org/10.1021/ja983494x

32. R. G. Parr, R. A. Donnelly, M. Levy, and W. E. Palke, J. Chem. Phys. **68**, 3801 (1978). https://doi.org/10.1021/ja004105d

33. P. K. Chattaraj and D. R. Roy, Chem. Rev. **107**, 64 (2007). https://doi.org/10.1021/cr078014b

34. A. Lesar and I. Milosev, Chem. Phys. Lett. **483**, 198 (2009). https://doi.org/10.1016/j.cplett.2009.10.082

35. N. R. Sheela, S. Muthu, and S. Sampathkrishnan, Spectrochim. Acta Part A: Mol. Biomol. Spectro. **120**, 237 (2014). https://doi.org/10.1016/j.saa.2013.10.007

36. R. Parthasarathi, V. Subramanian, D. R. Roy, and P. K. Chattaraj, Bioorg. Med. Chem. **12**, 5533 (2004). https://doi.org/10.1016/j.bmc.2004.08.013

37. D. A. Zainuri, I. A. Razak, and S. Arshad, Acta Cryst. E: **74**, 780 (2008). https://doi.org/10.1107/S2056989018006527

38. K. Arulaabaranam, S. Muthu, G. Mani, and S. Sevvanthi, J. Mol. Struct. **1220**, ID 128639 (2020). https://doi.org/10.1016/j.molstruc.2020.128639

39. Z. Zhou and H.V. Navangul, J. Phys. Org. Chem. **3**, 784 (1990). https://doi.org/10.1002/poc.610031203